From wild Lorenz-like to wild Rovella-like dynamics

Stefanie Hittmeyer, Bernd Krauskopf, Hinke M. Osinga
Department of Mathematics, The University of Auckland
Private Bag 92019, Auckland 1142, New Zealand

February 2015

Abstract

We consider a two-dimensional noninvertible map that was introduced by Bamón, Kiwi and Rivera as a model of a wild Lorenz-like attractor in a vector field of dimension at least five; such an attractor contains an expanding equilibrium and a hyperbolic set with robust homoclinic tangencies. Advanced numerical techniques enable us to study how the stable, unstable and critical sets of the map change within the conjectured region of wild chaos in the transition from Lorenz-like to Rovella-like dynamics, that is, when the equilibrium becomes contracting. We find numerical evidence for the existence of wild Rovella-like attractors, wild Rovella-like saddles and regions of multistability, where a Rovella-like attractor coexists with two fixed-point attractors. We identify bifurcations generating these different types of dynamics and compute them in two-parameter bifurcation diagrams.

1 Introduction

In 2006, Bamón, Kiwi and Rivera-Letelier [1] constructed an explicit two-dimensional noninvertible map as the reduction of a *wild Lorenz-like attractor* in a vector field of dimension $n \geq 5$. The term *wild* refers to the existence of a hyperbolic set that has robust homoclinic tangencies, that is, there are C^1-open sets of parameter values such that the corresponding hyperbolic set has a tangency between its stable and unstable manifolds. We refer to the existence of a wild hyperbolic set as *wild chaos*. This type of chaos can only exist in higher-dimensional systems, such as vector fields of dimension at least four, diffeomorphisms of dimension at least three or noninvertible maps of dimension at least two. The attractor is called *Lorenz-like*, because it is a higher-dimensional analogue of the *geometric Lorenz attractor* [2, 3, 4, 5], which is a geometric model of the attractor in the famous three-dimensional Lorenz system [6]. The dynamics on the Lorenz-like attractor in [1] can be reduced to the dynamics of the two-dimensional noninvertible map in a similar way as the dynamics on the geometric Lorenz attractor can be reduced to the one-dimensional noninvertible *Lorenz map*; see Section 2.1 for details. The two-dimensional noninvertible map constructed in [1] (for the special case $c = 1$) is given by

$$\begin{aligned} f : \mathbb{C}\backslash\{0\} &\to \mathbb{C}, \\ z &\mapsto (1 - \lambda + \lambda|z|^a)\left(\frac{z}{|z|}\right)^2 + c, \end{aligned} \tag{1}$$

with $c \in \mathbb{C}$, $a \in \mathbb{R}^+$ and $\lambda \in [0, 1]$. For $a < 1$ in (1), the attractor of the associated vector field is *expanding*, that is, it contains an equilibrium with one unstable eigenvalue $\lambda_u > 0$, and two stable eigenvalues $\lambda_{ss} < \lambda_{ws} < 0$ such that $-\lambda_{ws} < \lambda_u$, which is also true for the geometric Lorenz attractor.

One of the challenges in the study of wild chaos is that there are only very few concrete examples; see [7, 8] for an example of a three-dimensional diffeomorphism with wild chaos. More specifically, the map constructed in [1] is one of the few examples of a system with a wild Lorenz-like attractor that is given by an explicit formula; see [9, 10, 11] for other examples. The region of existence of the wild Lorenz-like attractor constructed in [1] is a very small region near the point $(a, \lambda) = (1, 1)$ for fixed $c = 1$. Our numerical investigations in [12] suggest that the region of existence of this attractor extends to a much larger set of parameter values $a, \lambda \in (0, 1)$ and for $c \in \mathbb{C}$. Furthermore, we found that the transition to wild chaos in this map is organised by a specific bifurcation structure consisting of infinite sequences of four types of tangency bifurcations; see Section 2.3. These bifurcations are interactions of different invariant sets that organise the dynamics of the map on the plane. These sets include the stable and unstable sets of a saddle fixed point, which are generalisations of stable and unstable manifolds in the setting of noninvertible maps, and the critical set, which arises due to the noninvertibility of the map; see Section 2.2. Continuation of these bifurcations shows that the mentioned bifurcation structure can be found along different routes into the region of existence of the wild Lorenz-like attractor; this is why we see it as the geometric mechanism for generating wild chaos in this map; see also [13].

In [14] Rovella studies a family of geometric Lorenz attractors that are *contracting* instead of expanding, that is, the eigenvalues of the equilibrium satisfy $-\lambda_{ws} > \lambda_u$; see also [15]. In [16] Araújo *et al.* study a higher-dimensional analogue, which can be reduced to a two-dimensional noninvertible map in a similar way as the vector field considered in [1]. The attractors constructed in [14, 15, 16] are referred to as contracting Lorenz attractors or *Rovella-like attractors*. The geometric Lorenz attractor and the higher-dimensional Lorenz-like attractor constructed in [1] are *robust*, that is, every sufficiently close vector field has a similar attractor nearby. In particular, these attractors are *robustly transitive*, which means that the attractor itself and all attractors of nearby vector fields contain a dense orbit. On the other hand, the Rovella attractor in [14] and the higher-dimensional Rovella-like attractor in [16] are non-robust in the sense that there are arbitrarily close vector fields that do not exhibit such an attractor. Nevertheless, they are *persistent* in the following way: each generic parametrised family of vector fields in certain sub-manifolds of the space of vector fields admits a positive Lebesgue measure set of parameter values that correspond to a vector field with a nearby transitive attractor. However, for a dense subset of nearby vector fields the attractor breaks down into one or two attracting periodic points and a hyperbolic set, with wandering orbits linking them [14].

In [1, 12, 13], the map is considered for the parameter $a := -\lambda_{ws}/\lambda_u < 1$, where the underlying attractor is Lorenz-like. In this paper, we study the map (1) in the transition from a wild Lorenz-like attractor for $a < 1$ to a wild Rovella-like attractor for $a > 1$. In particular, we want to find out whether, or in which form, the geometric ingredients for wild chaos persist and what new dynamical features appear during this transition. To address these questions, we study the changes of the stable, unstable and critical sets when the parameters are varied along a specific path in parameter space; importantly, this path stays within the region where we believe wild chaos exists. More specifically, we restrict to $c \in \mathbb{R}^+$ and represent the three-dimensional parameter space of $(c, a, \lambda) \in \mathbb{R}^+ \times \mathbb{R}^+ \times [0, 1]$ by four two-parameter bifurcation diagrams: those in the (a, λ)-plane for fixed $c = 0.1$ and fixed $c = 1$, and those in the (c, λ)-plane for fixed $a = 0.8$ and $a = 2$. We find that the bifurcation curves that bound the region of existence of wild chaos for $a < 1$, as conjectured in [12], extend to the region of $a > 1$. This suggests that wild chaos continues to exist even though the equilibrium in the underlying vector field changes from expanding to contracting, meaning that the associated attractor changes correspondingly

from a Lorenz-like to a Rovella-like attractor.

In order to understand what this means for the dynamics of the map (1), we choose a specific path of parameter values $(a, \lambda) \in (0, 2] \times [0, 1]$ for $c = 1$ that lies between the bifurcation curves that form the boundary of wild chaos for $a < 1$; along this path, a is monotonically increasing. We then study the changes in the invariant sets of (1) in the phase space when (a, λ) moves along this parameter path. We start in the corresponding parameter region for $a < 1$, in which the map (1) admits a wild Lorenz-like attractor. Here the stable, unstable and critical sets are entangled in a complicated way due to the tangency bifurcations generating wild chaos in the map (1) for $a < 1$. As a increases to $a > 1$, infinity becomes attracting in the map (1) and the *Julia set*, defined as the boundary of the basin of infinity, forms an additional invariant set of (1). In [17] we studied the map (1) for fixed $a = 2$, where it acts as a nonanalytic perturbation of the complex quadratic family $z \mapsto z^2+c$. We found that the four tangency bifurcations between the (un)stable and critical sets interact with the Julia set in novel ways that lead to drastic changes in the topology of the Julia set. For $a > 1$ on the chosen parameter path within the wild chaotic region, the Julia set coexists with the other invariant sets and the stable, unstable and critical sets maintain their geometric properties. However, now the dynamics is Rovella-like, and so we conjecture the existence of a wild Rovella-like attractor. As a increases further along the path, the invariant sets still have the same geometric properties, but two symmetric repelling fixed points turn into attractors in a Neimarck–Sacker bifurcation. These seem to be the only attractors and we find numerical evidence for the existence of a chaotic saddle, which we refer to as a *wild Rovella-like saddle*. We find that the disappearance of the wild Rovella-like attractor and the appearance of the wild Rovella-like saddle is caused by a boundary crisis of the Rovella-like attractor with a repelling invariant circle, which appears at the Neimarck–Sacker bifurcation. The parameter region between these bifurcations is a region of multistability, where the Rovella-like attractor coexists with the fixed-point attractors.

This paper is organised as follows. In Section 2, we discuss the basic properties and the Lorenz-like construction of the map (1). We then introduce the invariant sets that organise its dynamics in Section 2.2 and review the four types of tangency bifurcations and their meaning in the underlying vector field in the formation of wild chaos for $a < 1$ in Section 2.3. In Section 3, we investigate the transition from the wild Lorenz-like to Rovella-like dynamics by studying the corresponding regions in the bifurcation diagrams in parameter space, and then investigate in Section 3.2 the transitions in the phase portraits along the chosen parameter path. We end with a discussion in Section 4.

2 Background and notation

The map (1) acts on the plane by opening up the origin to a circle of radius $1-\lambda$, wrapping the plane twice around it and translating by c. Hence, it maps the punctured complex plane $\mathbb{C}\backslash\{0\}$ outside the disk $\overline{\mathbb{D}}_{1-\lambda}(c)$ in a 2-to-1 fashion. We call the origin $J_0 := \{0\}$ the *critical point* and the circle $J_1 := \partial\overline{\mathbb{D}}_{1-\lambda}(c)$ the *critical circle* of (1).

The map (1) is symmetric under rotation by 2π, that is, $f(z) = f(-z)$ for all z in $\mathbb{C}\backslash\{0\}$; for $c \in \mathbb{R}$ it is also symmetric under complex conjugation, that is, $f(z) = f(\overline{z})$ for all z in $\mathbb{C}\backslash\{0\}$. The points in the disk bounded by J_1 have no preimage, and the points outside this disk have two symmetric preimages given by

$$f_{0,1}^{-1}(z) := \pm \left(\frac{|z-c| - 1 + \lambda}{\lambda} \right)^{1/a} \sqrt{\frac{z-c}{|z-c|}}.$$

The k-th preimage $f^{-k}(z)$ of z consists of up to 2^k points, each of which is given as a sequence of preimages $f_{s_k}^{-1} \circ \cdots \circ f_{s_1}^{-1}(z)$ for $(s_l)_{1 \le l \le k} \in \{0,1\}^k$.

2.1 The Lorenz-like construction of the map

We now discuss the Lorenz-like nature of the map (1) as constructed in [1]. Let us first recall the construction of the *geometric Lorenz attractor* as an abstract geometric model of the Lorenz attractor in three-dimensional vector fields; see [2, 3, 4, 5, 18, 19]. An attractor of a three-dimensional vector field is a geometric Lorenz attractor if it has the following properties:

1. The attractor contains an equilibrium x that has eigenvalues $\lambda_{ss} < \lambda_{ws} < 0 < \lambda_u$ such that $-\lambda_{ws} < \lambda_u$.

2. The vector field admits a two-dimensional Poincaré section Σ, such that the Poincaré return map $\hat{f}$ defined on $\Sigma \backslash \hat{J}_0$ is a local diffeomorphism. The curve $\hat{J}_0$ consists of the points that go to x and do not return to Σ under the flow, that is, $\hat{J}_0$ is the last intersection of the stable manifold of x with Σ.

3. There is a one-dimensional stable invariant foliation on Σ that is uniformly contracted by $\hat{f}$. The intersection curves of the stable manifold of x lie dense in the leaves of this foliation and the quotient of Σ by this foliation is a compact interval I.

4. The quotient map of $\hat{f}$ acting on I is a one-dimensional noninvertible map f, which is discontinuous, has unbounded derivative at the critical point $J_0 := \hat{J}_0 \cap I$, and is smooth and uniformly expanding on $I \backslash \{J_0\}$. This one-dimensional map f is called the *Lorenz map*.

Tucker [20] proved that the attractor in the Lorenz system [6] (for the classical parameter values) has these properties and, therefore, that it is indeed a geometric Lorenz attractor.

Bamón, Kiwi and Rivera-Letelier [1] construct an analogue of the geometric Lorenz attractor in an n-dimensional vector field for $n \ge 5$. In order for this attractor to allow for richer dynamics than the geometric Lorenz attractor, the equilibrium has to have an unstable dimension of at least two. More precisely, they require the equilibrium to have eigenvalues $\lambda_{ss} < \lambda_{ws} < 0 < \lambda_u$, as in the geometric Lorenz attractor, but here, the multiplicity of λ_u is two and the multiplicity of λ_{ss} is $n-3$. Furthermore, in addition to the expanding condition $-\lambda_{ws} < \lambda_u$, they require $\lambda_u < -\lambda_{ss}$. In their construction, the Poincaré section Σ and the Poincaré return map $\hat{f}$ are $(n-1)$-dimensional, and the uniformly contracting foliation is $(n-3)$-dimensional. Correspondingly, the quotient map f of $\hat{f}$ by this foliation is a two-dimensional noninvertible map acting on the two-dimensional quotient space. This map is not defined at the critical point J_0 and the expanding condition means that it has unbounded derivative at J_0.

The Lorenz-like attractor in [1] is, in fact, constructed by extending the two-dimensional noninvertible map (1) for $c = 1$ and $a = -\lambda_{ws}/\lambda_u$ to an $(n-1)$-dimensional diffeomorphism $\hat{f}$ that is contracting on the other $n-3$ variables. This diffeomorphism is then suspended to yield an n-dimensional vector field in an abstract way; that is, in contrast to the Lorenz system, there is no formula for the vector field. In fact, for $n > 5$, the n-dimensional vector field is an embedding of the five-dimensional version into a transversally contracting five-dimensional submanifold of the n-dimensional space. Therefore, we will only consider the case $n = 5$ from now on.

2.2 Invariant sets

The dynamics of the map (1) on the plane is organised by several invariant sets. First of all there are the preimages of the critical point, which form the *backward critical set*

$$\mathcal{J}^- := \bigcup_{k\geq 0} f^- k(J_0),$$

and the images of the critical circle, which form the *forward critical set*

$$\mathcal{J}^+ := \bigcup_{k\geq 0} f^k(J_1);$$

together, they form the *critical set* $\mathcal{J} := \mathcal{J}^- \cup \mathcal{J}^+$. If one thinks of the critical circle J_1 as the multivalued image of the critical point J_0, then the critical set $\mathcal{J}$ is invariant under the map (1) and its inverse.

The critical point J_0 corresponds to the last intersection of the stable manifold of the equilibrium x with the Poincaré section Σ. Therefore, the backward critical set $\mathcal{J}^-$ corresponds to all intersections of this manifold with Σ, and correspondingly to the entire stable manifold of x for the underlying five-dimensional vector field. Similarly, the critical circle J_1 corresponds to the last intersection of the unstable manifold of the equilibrium x with the Poincaré section Σ in the Poincaré map, and the forward critical set corresponds to all intersections of this manifold with Σ and, thus, to the entire unstable manifold of x for the vector field.

Other important invariant sets are the *stable and unstable sets* of saddle fixed points and saddle periodic points; these are the generalisations of stable and unstable manifolds of saddle periodic orbits to the setting of noninvertible maps. For most of the parameter regions considered in this paper the map (1) admits a saddle fixed point p on the positive real axis, which corresponds to a saddle periodic orbit Γ of the underlying five-dimensional vector field; see [12] for details. Accordingly, the stable and unstable sets of p correspond to stable and unstable manifolds of Γ; by construction, these manifolds have dimensions four and two, respectively.

For a small enough neighbourhood V of p, we define the *local stable manifold* $W^s_{loc}(p)$ as

$$W^s_{\rm loc}(p) := \{z \in \mathbb{C} : f^k(z) \in V \text{ for all } k \geq 0\},$$

which is tangent to the stable eigenspace of p [21]. The *stable set* $W^s(p)$ is given by all preimages of $W^s_{loc}(p)$, that is,

$$W^s(p) := \bigcup_{k\geq 0} f^{-k}(W^s_{\rm loc}(p)).$$

Since the map (1) has two branches of preimages, $W^s(p)$ consists of infinitely many disconnected branches and, in particular, it is not an immersed manifold [22]. We call the branch containing p the *primary branch* $W^s_0(p) \supseteq W^s_{\rm loc}(p)$. For $c \in \mathbb{R}^+$, as considered in this paper, $W^s_0(p)$ is contained in the positive real axis, and for $c \in \mathbb{R}^+$ and $a < 1$ they coincide. In particular, $W^s_0(p)$ intersects the critical circle J_1 in the points $c \pm (1-\lambda)$ and, therefore, the points in $\mathcal{J}^-$ lie in the closure of $W^s(p)$. More specifically, they form the branch points of the set $W^s(p)$ in the sense that at least four branches of $W^s(p)$ connect at each point in $\mathcal{J}^-$; see already Section 3.2.

For a neighbourhood V of p, the *local unstable manifold* $W^u_{\rm loc}(p)$ is defined as the local stable manifold with respect to the local inverse $f^{-1}_{\rm loc}$ of the map (1) that satisfies $f^{-1}_{\rm loc}(p) = p$, that is,

$$W^u_{\rm loc}(p) := \{z \in \mathbb{C} : (f^{-1}_{\rm loc})^k(z) \in V \text{ for all } k \geq 0\},$$

which is tangent to the unstable eigenspace at p. The *unstable set* $W^u(p)$ is given by all images of the local unstable manifold $W^u_{\text{loc}}(p)$, that is,

$$W^u(p) := \bigcup_{k\geq 0} f^k(W^u_{\text{loc}}(p)).$$

For a diffeomorphism, the set $W^u(p)$ is an immersed manifold, but for the noninvertible map (1) it is a single continuous curve that may have self-intersections at points $z \in W^u(p)$ for which both preimages $f_0^{-1}(z)$ and $f_1^{-1}(z)$ lie in $W^u(p)$.

For $a < 1$, infinity can be viewed as a repelling fixed point of (1), while for $a > 1$ it is an attractor. Therefore, for $a > 1$, there is an additional invariant set, namely the *Julia set* $\mathcal{Y}$, which we define as the boundary of the basin of attraction of infinity, that is,

$$\mathcal{Y} := \partial\mathcal{B}(\infty).$$

The set $\mathcal{Y}$ is a chaotic repellor and repelling (pre-)periodic points appear to be dense in it; see [17] for details. In the underlying five-dimensional vector field, the suspension of Julia set $\mathcal{Y}$ is a chaotic saddle, but its exact role in this setting is still unknown. In particular, it remains an interesting question for future research when and in which way its stable manifold bounds the basin of the Rovella-like attractor in the vector field.

In order to study the changes in the dynamics of the map (1), we consider the changes in the geometry of the fixed points and the invariant sets $W^s(p)$, $W^u(p)$, $\mathcal{J}$ and $\mathcal{Y}$, which organise the dynamics on the plane. For each (c, a, λ), we refer to the representation of these sets as the *phase portrait* of the map (1). In order to be able to study the phase portraits globally on the entire plane, we project it onto the Poincaré disk via the stereographic transformation

$$\begin{aligned} T : \mathbb{C} \cup \{\infty\} &\to \overline{\mathbb{D}}_1(0) \\ z &\mapsto \frac{z}{1+|z|}. \end{aligned} \tag{2}$$

This transformation maps the origin to itself and infinity onto the unit circle.

2.3 Tangency bifurcations

The following four types of tangency bifurcations between the stable and unstable sets $W^s(p)$ and $W^u(p)$ and the forward and backward critical sets $\mathcal{J}^+$ and $\mathcal{J}^-$ play a crucial role in the transition to wild chaos in the map (1). These are quadratic tangencies of respective objects and, hence, they are of codimension one; see [12, 13] for more details and illustrations.

- *Homoclinic tangencies*: the stable and unstable sets $W^s(p)$ and $W^u(p)$ are tangent. There is a first homoclinic tangency, which entails an infinite sequence of homoclinic tangencies accumulating on each other. After the first homoclinic tangency, the sets $W^s(p)$ and $W^u(p)$ form a homoclinic tangle and $W^u(p)$ accumulates on itself. A homoclinic tangency in the map (1) corresponds to a homoclinic bifurcation of the equilibrium x in the underlying vector field.

- *Forward critical tangencies*: the stable set $W^s(p)$ and the forward critical set $\mathcal{J}^+$ are tangent and, as a result, branches of $W^s(p)$ connect up at the points in the backward critical set $\mathcal{J}^-$. There is no first forward critical tangency, but an infinite sequence of forward critical tangencies accumulating on each homoclinic tangency. Therefore, immediately after the first homoclinic tangency, $W^s(p)$ has reconnected at the points in $\mathcal{J}^-$ in such a way, that it accumulates on itself. A forward critical tangency in (1) corresponds to a heteroclinic bifurcation that connects x to the periodic orbit Γ in the vector field.

- *Backward critical tangencies*: a sequence of points in the backward critical set $\mathcal{J}^-$ lies on the unstable set $W^u(p)$, and images of the corresponding curve segments in $W^u(p)$ form cusps at the circles in the forward critical set $\mathcal{J}^+$. There is a first backward critical tangency, which entails an infinite sequence of backward critical tangencies accumulating on each other. After the first backward critical tangency, $W^u(p)$ forms loops around all circles in $\mathcal{J}^+$. A backward critical tangency in (1) corresponds to a heteroclinic bifurcation that connects Γ to x in the vector field.

- *Forward-backward critical tangencies*: a sequence of points in the backward critical set $\mathcal{J}^-$ lies in the forward critical set $\mathcal{J}^+$, and images of the corresponding curve segments in $\mathcal{J}^+$ form cusps at the circles in $\mathcal{J}^+$. There is no first forward-backward critical tangency, but an infinite sequence of forward-backward critical tangencies accumulating on each backward critical tangency. Therefore, immediately after the first backward critical tangency, $\mathcal{J}^+$ forms infinitely many loops around all its circles. There is a last forward-backward critical tangency, given by $|c| = 1 - \lambda$, when the critical point J_0 lies on the critical circle J_1 and all preimages of J_0 in $\mathcal{J}^-$ disappear into J_0. A forward-backward critical tangency gives rise to periodicity of the critical set $\mathcal{J}$ in the following sense: if J_0 is contained in the disk bounded by a circle $J_k \subset \mathcal{J}^+$ then there is a point in $J_{-k+1} \in \mathcal{J}^-$ that lies in the disk bounded by J_1. If one thinks of this point as the image of J_0, the point J_0 is k-periodic. Hence, a forward-backward critical tangency in the map (1) corresponds to a homoclinic bifurcation of the periodic orbit Γ in the vector field.

Homoclinic tangencies are also encountered in diffeomorphisms, but the three tangency bifurcations of the critical set $\mathcal{J}$ are related to the noninvertibility of the map (1). The first homoclinic tangency is the onset of (regular) chaos in (1), in the sense that it is the same mechanism that generates chaos in diffeomorphisms. After this bifurcation, the closure $\overline{W^u(p)}$ of the unstable set $W^u(p)$ forms a chaotic attractor. In [12] we conjecture that the first backward critical tangency forms the onset of wild chaos in the map (1) for $a < 1$, and $\overline{W^u(p)}$ becomes a wild Lorenz-like attractor. Immediately after this bifurcation all four types of tangency bifurcations have occurred in infinite sequences, leading to the complicated accumulation of the sets $W^s(p)$, $W^u(p)$, $\mathcal{J}^-$ and $\mathcal{J}^+$. In the underlying vector field, this corresponds to a complicated accumulation of homoclinic and heteroclinic connections between the periodic orbit Γ and the equilibrium x, which lie in the same hyperbolic set. Therefore, we see this bifurcation structure as the geometric mechanism generating wild chaos in this system.

3 Transition from wild Lorenz-like to wild Rovella-like dynamics

We now study the changes in the dynamics, when the expanding condition $-\lambda_{ws} < \lambda_u$ in the construction of Lorenz-like attractor, discussed in Section 2.1, is replaced by the contracting condition $-\lambda_{ws} > \lambda_u$. In terms of the map (1), this means that the parameter $a = -\lambda_{ws}/\lambda_u$ is increased from $a < 1$ to $a > 1$. We start by investigating four two-parameter bifurcation diagrams in the (c, a, λ)-space in Section 3.1, and then study in Section 3.2 the changes to the phase portrait along a specific curve through parameter space. The transition from Rovella-like attractor to saddle-type dynamics is the subject of Section 3.3.

3.1 Bifurcation diagrams

Figure 1 is an illustration of the bifurcation structure of the map (1) in the (c, a, λ)-space. Panel (a) shows how the bifurcation diagrams in the four planes defined by $a = 0.8$, $a = 2$, $c = 0.1$ and $c = 1$ intersect each other in (c, a, λ)-space. The light-grey curves denote $a = 0.8$, $a = 1$, $c = 0.1$ and $c = 1$, at which the four planes intersect. Panels (b)–(e) show the corresponding two-parameter bifurcation diagrams in the (a, λ)-plane for $c = 1$ and $c = 0.1$, and in the (c, λ)-plane for $a = 2$ and $a = 0.8$, respectively. We computed these bifurcation diagrams by formulating the bifurcation conditions as boundary conditions for appropriate boundary value problems and continuing the solutions in two parameters with Cl_MatContM [23, 24, 25]; see [12] for details.

In Figure 1, the curve labelled L is a curve of saddle-node bifurcations at which the saddle fixed point p meets a repelling fixed point s on the real line and disappears; the points p and s only exist for parameter values to the left of L in panels (b) and (d), and below the lower segment and above the upper segment of L in panel (c). At the line defined by $a = 1$ in panels (b) and (c) the point s appears at infinity; it only exists for $a > 1$. One could think of this bifurcation as a branch point and we denote it by BP. In fact, infinity becomes attracting for $a > 1$ and the Julia set $\mathcal{Y}$ appears at infinity as its basin boundary. More precisely, at the same time when s appears at infinity, infinitely many other repelling periodic points appear at infinity as well, and their closure coincides with $\mathcal{Y}$; see [17]. The curves labelled BP and L both emanate from the point $(a, \lambda) = (1, 1)$. The curve labelled P is a curve of pitchfork bifurcation of the fixed point p, where two complex-conjugate fixed points q^+ and $q^- = \overline{q^+}$ appear near p in the upper and lower half-plane, respectively; for parameter values above P in panels (d) and (c) and below P in panel (e) p is an attractor and $q^\pm$ do not exist; for parameter values on the other side of P, the fixed point p is a saddle and $q^\pm$ are attractors initially. The curve labelled NS is a curve of Neimarck–Sacker bifurcations of the fixed points q^+ and q^-; these are repellors for parameter values above NS in panels (b), (d) and (e) and below NS in panel (c); for parameter values on the other side of NS they are attractors. The line labelled FB is the curve of last forward-backward critical tangencies, given by $|c| = 1 - \lambda$; for parameter values below FB the critical point J_0 lies inside the disk bounded by the critical circle J_1; therefore, J_0 does not have any preimages and the backward critical set $\mathcal{J}^-$ consists of J_0 only; for parameter values above FB the critical point J_0 lies outside the disk bounded by J_1 and $\mathcal{J}^-$ contains infinitely many points accordingly. In addition, the fixed points $q^\pm$ only exist above FB and disappear into J_0 when $|c| = 1 - \lambda$.

The curves labelled H and B in Figure 1 are the curves of first homoclinic and first backward critical tangencies, respectively. The stable and unstable sets $W^s(p)$ and $W^u(p)$ form a homoclinic tangle for parameter values to the right of H in panel (b) and to the left of H in panels (c)–(e). Similarly, the unstable set $W^u(p)$ forms loops around the circles in the forward critical set $\mathcal{J}^+$ for parameter values to the right of B in panel (b) and to the left of B in panels (c)–(e), respectively. Note that H and B lie on the sides of L for which the saddle point p exists. Similarly, NS lies on the sides of FB, for which the points $q^\pm$ exist, and P lies on the sides of L and FB, for which both p and $q^\pm$ exist. The curves NS, P and FB emanate from the points $(c, \lambda) = (0, 1)$ and $(c, \lambda) = (0.25, 1)$ in panel (d), and from the same point $(c, \lambda) = (1, 0)$ in panel (e), respectively. Hence, these points form organising centres for the bifurcation diagram in the (c, λ)-plane.

We conjecture in [12] that the first homoclinic and the first backward critical tangency are responsible for the onset of wild chaos for $a < 1$. These geometric ingredients of wild chaos are also present in the region bounded by B, BP and L in Figure 1(b), and the regions bounded by B, FB and L in Figure 1(c) and (d). For $a > 1$ in these regions, the

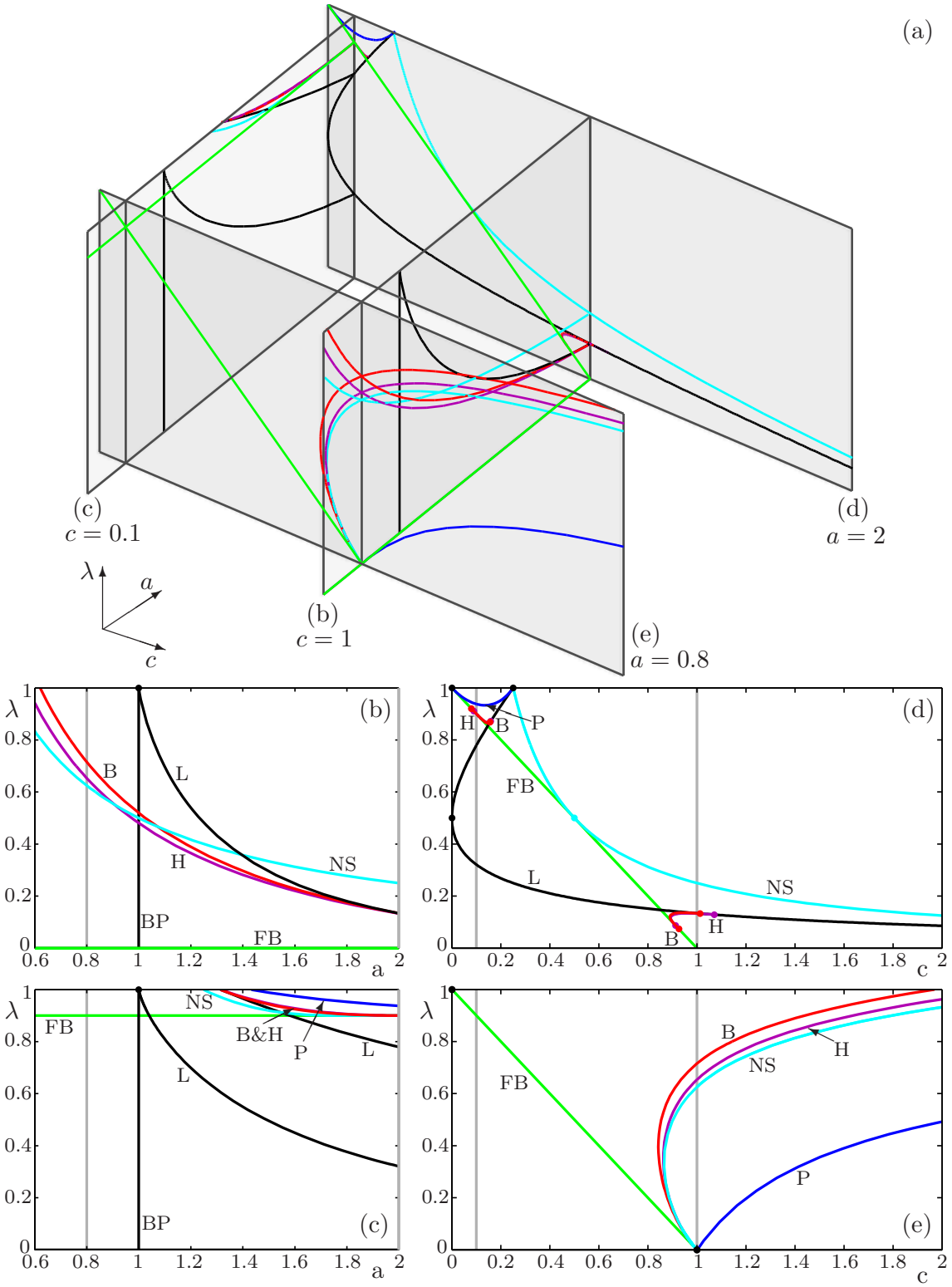

Figure 1: The organisation of (c, a, λ)-space (a), as represented by bifurcation diagrams in the (a, λ)-plane for $c = 1$ (b) and $c = 0.1$ (c), and in the (c, λ)-plane for $a = 2$ (d) and $a = 0.8$ (e). Shown are curves of saddle-node bifurcations (L, black), of branch point bifurcations (BP, black), of pitchfork bifurcations (P, blue), of Neimarck–Sacker bifurcations (NS, cyan), of last forward-backward critical tangencies (FB, green), of first homoclinic tangencies (H, purple), and of first backward critical tangencies (B, red). The respective planes intersect in the grey vertical lines.

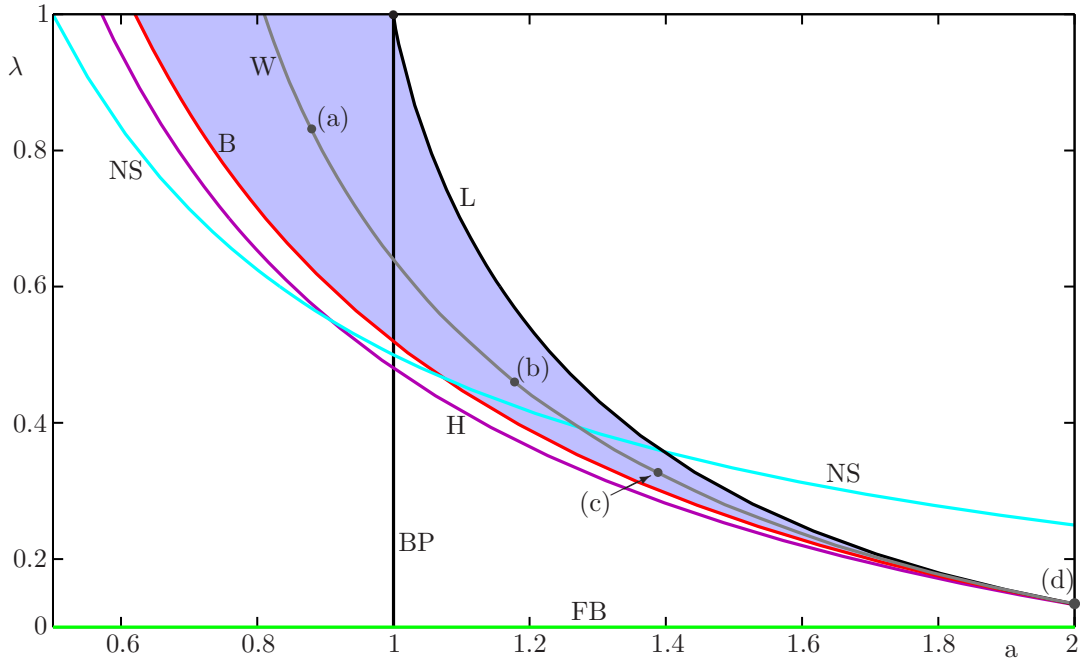

Figure 2: The bifurcation diagram in the (a, λ)-plane for fixed $c = 1$ from Figure 1(b); also shown is the conjectured region of wild chaos (shaded blue) and the path W (grey) with selected parameter points (a)–(d).

equilibrium x of the underlying vector field is no longer expanding; hence, the dynamics is no longer Lorenz-like, but Rovella-like. This suggests the existence of wild Rovella-like dynamics in these parameter regions.

3.2 Dynamics along a parameter path

We now investigate the transition of the phase portrait of the map (1) as the parameters a and λ are moved along a path within the (conjectured) wild chaotic region, where $c = 1$ fixed. Figure 2 shows an enlargement of the bifurcation diagram from Figure 1(c); we shaded the parameter region between B and L where wild chaos is conjectured to exist. The curve W is the parameter path within this region along which we investigate the changes in the phase portraits of (1); the path W lies half-way between B and L. The points on W labelled (a)–(d) are chosen to illustrate the different regions for the dynamics and Figure 3 shows the associated four phase portraits. In Figure 3 we plot the saddle fixed points p and the repelling fixed point s on the positive real axis; the fixed points q^+ and q^- in the upper and lower half-planes, respectively; the stable set $W^s(p)$ up to the 8-th preimage of the primary branch $W_0^s(p)$; the unstable set $W^u(p)$ up to arclength 10 on each side of p; the backward critical set $\mathcal{J}^-$ up to the 6-th preimage of the critical point J_0; the forward critical sets $\mathcal{J}^+$ up to the 8-th image of the critical circle J_1; and the Julia set $\mathcal{Y}$ as the boundary of the basin of attraction of infinity.

Figure 3(a) shows the phase portrait of (1) for $(a, \lambda) = (0.88, 0.83)$, which is in the conjectured region of existence of the wild Lorenz-like attractor. Infinity is repelling and p, q^+ and q^- are the only fixed points; p is a saddle and $q^\pm$ are repellors. The stable and unstable sets $W^s(p)$ and $W^u(p)$ form a homoclinic tangle. The set $W^s(p)$ has infinitely many branches, formed by the preimages of the primary branch $W_0^s(p)$, which is the positive real line. Every branch of $W^s(p)$ is accumulated by an infinite sequence of other branches in $W^s(p)$. The sets $W^u(p)$ and $\mathcal{J}^+$ form infinitely many loops around the circles in the

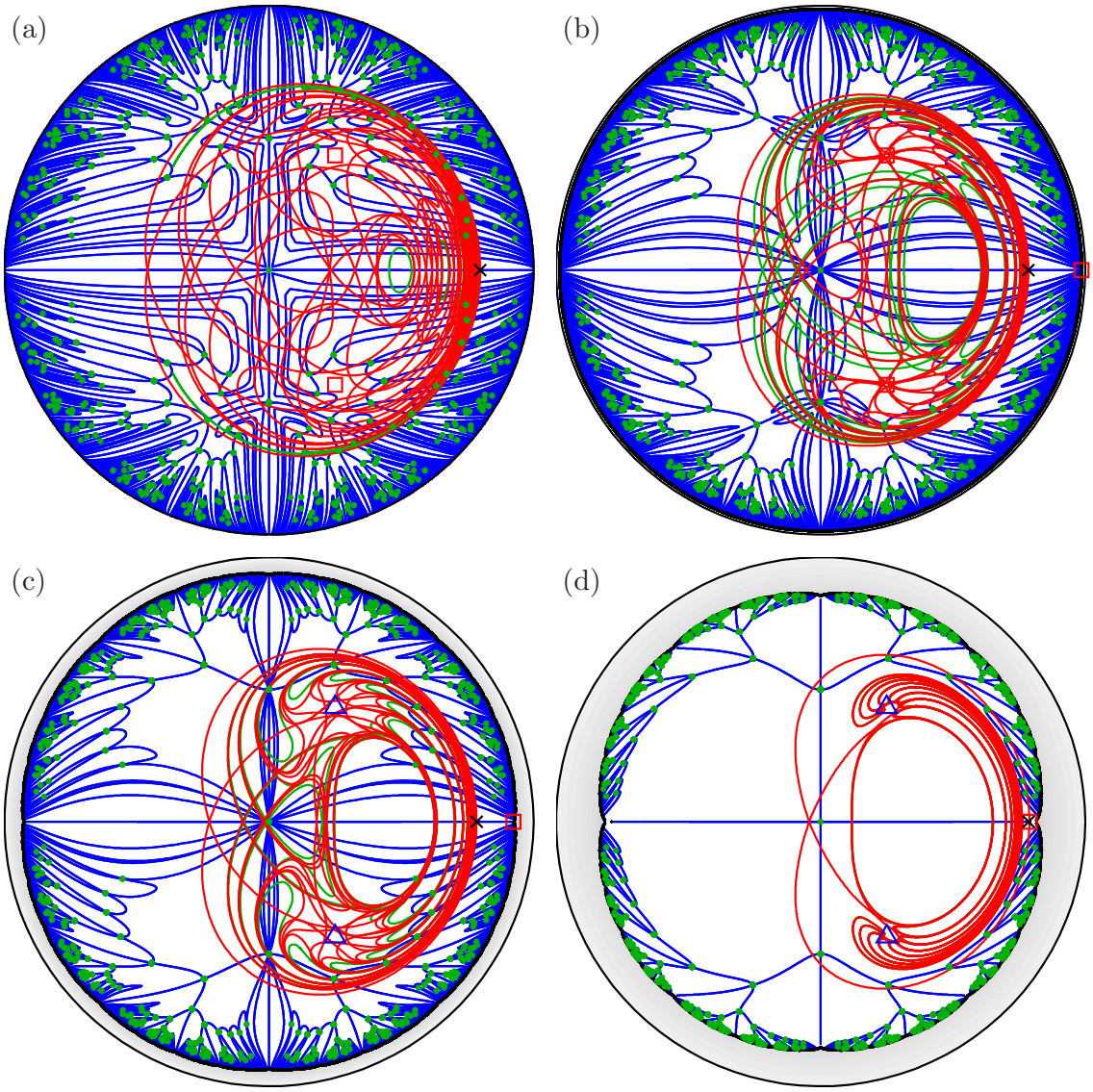

Figure 3: Phase portraits for the parameter points labelled (a)–(d) on the path W in Figure 2, namely, for $(a, \lambda) = (0.88, 0.83)$ in (a), $(a, \lambda) = (1.178, 0.46)$ in (b), $(a, \lambda) = (1.38, 0.32)$ in (c), and $(a, \lambda) = (2, 0.13)$ in (d). Shown are the fixed points p (black cross), s (red square) and $q^{\pm}$ (red squares when repelling, blue triangles when attracting), the stable set $W^s(p)$ (blue curves), the unstable set $W^u(p)$ (red curve), the backward critical set $\mathcal{J}^-$ (green dots), the forward critical set $\mathcal{J}^+$ (green curves), the Julia set $\mathcal{Y}$ (black) and the basin of attraction of infinity (grey).

forward critical set $\mathcal{J}^+$. Numerical simulations (not shown) suggest that the closure $\overline{W^u(p)}$ of the unstable set $W^u(p)$ is, in fact, a chaotic attractor, which we denote $\mathcal{A}$; its basin of attraction $\mathcal{B}(\mathcal{A})$ is the entire punctured plane except for the points $q^{\pm}$. Indeed, we conjecture that $\mathcal{A}$ is a wild Lorenz-like attractor [12].

Figure 3(b) shows the phase portrait for $(a, \lambda) = (1.178, 0.46)$. Since $a > 1$, infinity is now attracting and admits a basin of attraction; the Julia set $\mathcal{Y}$ is its basin boundary. The repelling fixed point s has appeared at infinity and lies in $\mathcal{Y}$. The branches of $W^s(p)$ do not go to infinity any longer, but end at preimages of s on $\mathcal{Y}$. Moreover, pre-periodic repelling points appear to lie dense in $\mathcal{Y}$. Nevertheless, $\mathcal{Y}$ does not coincide with the closure of all (pre-)periodic repelling points, because the repelling fixed points $q^{\pm}$ lie far away from $\mathcal{Y}$. We note that the geometric ingredients of wild chaos that we identified are still present: the sets $W^s(p)$ and $W^u(p)$ form a homoclinic tangle and accumulate on themselves, $W^u(p)$ forms infinitely many loops around the circles in $\mathcal{J}^+$, and the circles in $\mathcal{J}^+$ form infinitely many loops around other circles in $\mathcal{J}^+$. The chaotic attractor $\mathcal{A} = \overline{W^u(p)}$ still seems to be present, but now its basin $\mathcal{B}(\mathcal{A})$ is bounded by $\mathcal{Y}$ and $q^{\pm}$. Figure 3(b) seems to suggest that $\overline{W^u(p)}$ is a wild Rovella-like attractor, that is, the corresponding attractor in the underlying vector field contains a contracting equilibrium and a hyperbolic set with robust homoclinic tangencies. However, we cannot rule out the possibility that there are periodic attractors of very high period in which case the set $\overline{W^u(p)}$ is not necessarily a chaotic attractor; then $\overline{W^u(p)}$ could contain a chaotic saddle, that is, a chaotic hyperbolic set of the map (1), such that each point in this set admits onedimensional stable and unstable sets; see the discussion in Section 4.

The transition of the chaotic attractor $\mathcal{A}$ from a wild Lorenz-like attractor in Figure 3(a) to a wild Rovella-like attractor in Figure 3(b) occurs when the parameter a crosses the line $a = 1$ within the wild chaotic region; we will discuss the persistence of the emerging Rovella-like attractor in more detail in Section 4.

Figure 3(c) shows the phase portrait for $(a, \lambda) = (1.38, 0.32)$. The basin of attraction of infinity has increased, and the fixed points p and $s \in \mathcal{Y}$ have moved closer together on the real line. The fixed points $q^{\pm}$ have turned into attractors at the Neimarck–Sacker bifurcation NS at $(a, \lambda) \approx (1.2738, 0.3925)$; see the bifurcation diagram in Figure 2. The fixed points $q^{\pm}$ are the only attractors in Figure 3(c) and their basins of attraction are bounded by $\overline{W^s(p)}$. In particular, the set $\overline{W^u(p)}$ now contains the attractors $q^{\pm}$ and does no longer form a chaotic attractor. Numerical simulation (not shown) suggests that $\overline{W^u(p)}$ now contains a chaotic saddle $\mathcal{S}$. The set $\mathcal{S}$ is given by the closure of all saddle periodic points, and its stable and unstable sets contain the stable and unstable sets of the saddle periodic points, respectively. More specifically, this means that $\overline{W^u(p)} = \overline{W^u(\mathcal{S})}$. Therefore, the set $W^u(p)$ illustrates the geometry of $\mathcal{S}$ in Figure 3(c). Since the geometric ingredients of wild chaos in terms of the geometric properties of the sets $W^u(p)$, $W^s(p)$, $\mathcal{J}^-$ and $\mathcal{J}^+$ are still present, we refer to $\mathcal{S}$ as a wild Rovella-like saddle. Note that the term wild refers to properties of an associated hyperbolic set in the vector field, which is not necessarily contained in an attractor.

Figure 3(d) shows the phase portrait for $(a, \lambda) = (2, 0.13)$. We note that the geometric properties of the sets $q^{\pm}$, $W^u(p)$, $W^s(p)$, $\mathcal{J}^-$ and $\mathcal{J}^+$ are still as in panel (c), and, therefore, we still conjecture the existence of the wild Rovella-like saddle $\mathcal{S}$. However, the branches of $W^s(p)$, the segments in $W^u(p)$ and the two fixed points p and s on the real line now lie very close together. This can be explained by the fact that near $(a, \lambda) = (2, 0.13)$ the curves of first homoclinic tangency H, first backward critical tangency B and saddle-node bifurcation L lie very close together; see Figure 2.

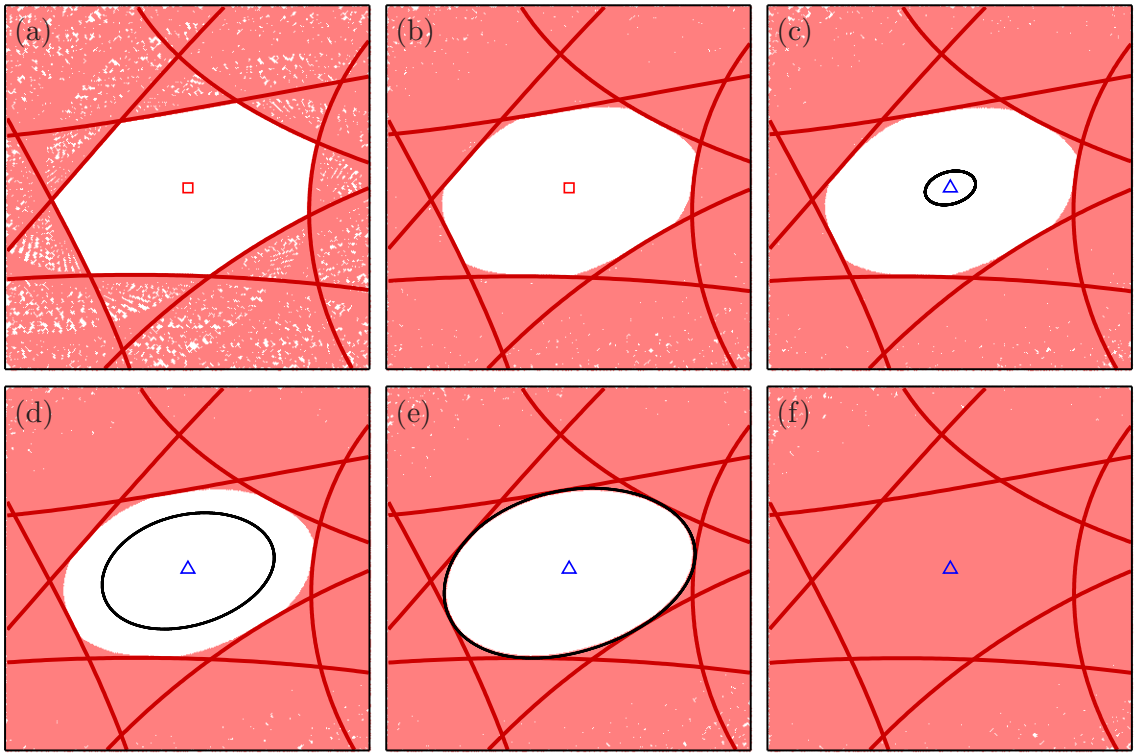

Figure 4: Phase portraits in the box $[0.21, 0.29] \times [0.393, 0.473]$ for $(a, \lambda) = (1.2718, 0.3939)$, $(a, \lambda) = (1.2738, 0.39259)$, $(a, \lambda) = (1.2739, 0.39248)$, $(a, \lambda) = (1.2741, 0.39236)$, $(a, \lambda) = (1.2744, 0.39221)$, and $(a, \lambda) = (1.2746, 0.39206)$ in panels (a)–(f), respectively. Shown are the fixed point q^+ (red square when repelling, blue triangle when attracting), segments (red curves) of the unstable set $W^u(p)$, points (light red) in the higher-order preimages of these segments and the repelling invariant circle $\mathcal{C}^+$ (black curve).

3.3 Role of the Neimarck–Sacker bifurcation

We now consider in more detail the transition between a wild Rovella-like attractor $\mathcal{A}$ and a wild Rovella-like saddle $\mathcal{S}$. One may conclude that this transition occurs when a crosses NS, but the Neimarck–Sacker bifurcation is a local bifurcation of the fixed points $q^{\pm}$, which does not affect the Rovella-like set. The transition from attractor to a saddle occurs, in fact, for parameter values very close, but to the right of NS. To this end, we study $W^u(p)$ — illustrating the attractor $\mathcal{A}$ and the saddle $\mathcal{S}$ as explained above — in a small region of phase space near the fixed point q^+; similar dynamics occurs at the complex-conjugate point q^-. Figure 4 illustrates the situation for six parameter values $(a, \lambda) \in \mathrm{W}$ very close to NS. We plot the fixed point q^+, segments of the unstable set $W^u(p)$, and, in panels (c)–(e) only, a repelling invariant circle $\mathcal{C}^+$ born at the Neimarck–Sacker bifurcation NS. We also show many additional points in $W^u(p)$ that are computed as higher-order preimages of the shown segments of $W^u(p)$; these points constitute a good approximation of $\overline{W^u(p)}$.

Figures 4(a) and (b) show the situation before the Neimarck–Sacker bifurcation at $(a, \lambda) = (1.2718, 0.3939)$ and $(a, \lambda) = (1.2738, 0.39259)$, respectively; the fixed point q^+ is a repellor and $\mathcal{A} = \overline{W^u(p)}$ seems to be a wild Rovella-like attractor; its basin of attraction $\mathcal{B}(\mathcal{A})$ is the entire punctured plane except for the points $q^{\pm}$ and their preimages, which form the basin boundary $\partial\mathcal{B}(\mathcal{A})$. The attractor $\mathcal{A}$ has a hole near q^+ given by the open bounded region (white) of points near q^+ that do not lie in $\mathcal{A}$; this hole coincides with the union of the point q^+ and the set $\mathcal{B}(\mathcal{A})\backslash\mathcal{A}$ near q^+. Note that the hole is bounded by

$W^u(p)$, as illustrated in panel (a); in panel (b), on the other hand, some of the higher-order preimages of the segments in $W^u(p)$ now lie closer to q^+, but $\mathcal{A}$ is still bounded away from q^+ and the boundary is formed by higher-order images of the segments of $W^u(p)$.

Figures 4(c) and (d) show the situation just after the Neimarck–Sacker bifurcation for $(a, \lambda) = (1.2739, 0.39248)$ and $(a, \lambda) = (1.2741, 0.39236)$, respectively. The point q^+ is now an attractor and, since the Neimarck–Sacker bifurcation is subcritical, a repelling invariant circle, which we denote $\mathcal{C}^+$, has appeared around q^+. The open disk bounded by $\mathcal{C}^+$ forms the immediate basin of q^+, whereas points in the hole of $\mathcal{A}$ and outside the disk bounded by $\mathcal{C}^+$ are in $\mathcal{B}(\mathcal{A})\backslash\mathcal{A}$. More precisely, the basin boundary $\partial\mathcal{B}(\mathcal{A})$ is now formed by $\mathcal{C}^+$, its complex-conjugate $\mathcal{C}^- := \overline{\mathcal{C}^+}$ and all their preimages. As was the case before, we cannot rule out the existence of periodic attractors of higher periods but our numerical observations suggest that set $\mathcal{A} = \overline{W^u(p)}$ is still a wild Rovella-like attractor, which now co-exists with the attractors $q^\pm$.

As shown in Figure 4(e), at $(a, \lambda) \approx (1.2744, 0.39221)$, the wild Rovella-like attractor $\mathcal{A}$ meets the invariant circle $\mathcal{C}^+$. This bifurcation is a *boundary crisis* of $\mathcal{A}$, because $\mathcal{C}^+$ lies in its basin boundary $\partial\mathcal{B}(\mathcal{A})$. At the moment of bifurcation, the open disk bounded by $\mathcal{C}^+$ still forms the immediate basin of q^+, which now coincides with the hole in $\mathcal{A}$. Hence, the set $\mathcal{B}(\mathcal{A})\backslash\mathcal{A}$ is now empty near q^+. We remark here that the boundary crisis is likely induced by a tangency between $W^u(p)$ and the stable manifold of a periodic orbit on $\mathcal{C}^+$ that has a very high period, that is, the circle $\mathcal{C}^+$ is no longer quasiperiodic; the precise nature of the dynamics on $\mathcal{C}^+$ is beyond the scope of this paper and we refer to [26, 27] for more details.

Figure 4(f) shows the situation at $(a, \lambda) = (1.2746, 0.39206)$, that is, after the boundary crisis bifurcation. The invariant circle $\mathcal{C}^+$ and the hole in $\overline{W^u(p)}$ have disappeared. Now all points in the shown region, including the segments and points in $W^u(p)$, lie in the immediate basin of the attractor q^+. Therefore, $\overline{W^u(p)}$ now contains the fixed-point attractor q^+, which means that the chaotic attractor $\mathcal{A}$ formed by $\overline{W^u(p)}$ has disappeared. Globally, the fixed points q^+ and q^- seem to be the only attractors, but there could also be higher-periodic attractors; see the discussion in Section 4. In the case that $q^\pm$ are the only attractors, their basins are bounded by $\overline{W^s(p)} = W^s(\mathcal{S})$; see Figures 3(c) and (d). However, the set $\overline{W^u(p)}$ now seems to contain a chaotic saddle $\mathcal{S}$, which is formed by the closure of infinitely many saddle periodic points. These points attract the points in their stable sets, but eventually repel all other points. In particular, the saddle fixed point p lies in $\mathcal{S}$ and $\overline{W^u(p)} = \overline{W^u(\mathcal{S})}$, as explained in Section 3.2, so we can see $W^u(p)$ as an illustration of a wild Rovella-like saddle $\mathcal{S}$. As a result, most points follow the 'ghost' of the former chaotic attractor $\overline{W^u(p)}$ for many iterations, but eventually converge to one of the attractors q^+ or q^-; this phenomenon is called *transient chaos* [28, 29].

4 Discussion

We investigated the dynamics of the map (1) when the equilibrium of the underlying vector field changes from expanding to contracting and the corresponding dynamics changes from Lorenz-like to Rovella-like. In [12] we conjectured that the region of existence of wild chaos for $a < 1$ is bounded by curves of first backward critical tangencies, saddle-node bifurcations and the line $\lambda = 1$. We presented two-parameter bifurcation diagrams that show how these bifurcation curves extend to the region of the Rovella-like dynamics for $a > 1$ in this map. Phase portraits along a path within the conjectured parameter region of wild chaos illustrate the transition from a wild Lorenz-like attractor for $a < 1$, via a wild Rovella-like attractor for $a > 1$ to a wild Rovella-like saddle for $a > 1$. The latter transition involves a Neimarck–Sacker bifurcation, a boundary crisis and a small region of

multistability between them.

The transition from wild Lorenz-like to wild Rovella-like dynamics in the map (1) is reminiscent of the transition from simple to chaotic dynamics in the original three-dimensional Lorenz system as the parameter ρ is increased; see [29, 30]. More specifically, for small ρ after a first homoclinic bifurcation, there is a region of *preturbulence* due to a chaotic saddle: all points outside the stable manifold of this saddle eventually go to one of two attracting equilibria after possibly very long transients. A chaotic attractor then appears at a heteroclinic bifurcation, which induces a boundary crisis; then one finds a region of multistability, where the chaotic attractor coexists with the attracting equilibria, before these become repelling in a Hopf bifurcation and the chaotic attractor is the only attractor. We find a corresponding bifurcation structure in the map (1) when a is decreased along the chosen path: first there is a wild chaotic saddle and two attracting fixed points; the wild chaotic attractor appears at a boundary crisis, followed by a region of multistability, before the attracting fixed points become repelling in a Neimarck–Sacker bifurcation and the wild chaotic attractor is the only attractor.

We conjecture that a wild Rovella-like attractor exists in the map (1). Further analytical investigations and detailed numerical studies would be necessary to provide evidence that it is persistent and non-robust as is the case for the Rovella attractor studied in [14] and the higher-dimensional Rovella-like attractor studied in [16]. In particular, there could be higher-periodic attractors within the conjectured region of wild chaos for $a > 1$ already above the curve NS. If these exist, we would expect that these periodic attractors undergo the same transition as the fixed-points attractors $q^{\pm}$. Namely, we would expect that they appear in Neimarck–Sacker bifurcations, followed by small regions of multistability, where they coexist with a wild Rovella-like attractor that turns into a wild Rovella-like saddle at a boundary crisis. However, other bifurcations could also be involved in the (dis-)appearance of these attractors. We searched for these periodic attractors in the vicinity of forward-backward critical tangencies of the map (1), because these bifurcations correspond to (dis-)appearing periodicity in the critical set; an example is the last forward-backward critical tangency, at which the points $q^{\pm}$ disappear at the critical point. However, above the curve NS, we find periodic saddles and repellors only; below NS we also found higher-periodic attractors, but these seem to disappear in a sequence of period-doubling bifurcations as one moves the parameters towards NS. The difficulty is that higher-periodic attractors — if they even exist above NS — would be of very high period and would only exist in very small parameter regions.

Another interesting question for future research is to study in more detail the consequences for the underlying vector field of interactions of the Julia set and the wild Rovella-like attractor in the map (1). These two sets correspond to hyperbolic sets with different stable dimensions in the vector field. In particular, the repelling periodic points in the Julia set and saddle periodic points in the attractor correspond to saddle periodic orbits with stable manifolds of dimensions three and four, respectively. Therefore, their interactions could lead to the formations of so-called *heterodimensional cycles*, that is, heteroclinic cycles between hyperbolic sets with different stable dimensions; this phenomenon is also referred to as a heteroclinic cycle with *unstable dimension variability* [31]. It is expected that the concept of *robust heterodimensional cycles* is related to the creation of wild chaos [32, 33, 34, 35]; see [36] for an introduction to the overall topic of *robust non-hyperbolicity*.

Another approach to study the involvement of heterodimensional cycles and wild chaos in the formation of robust non-hyperbolicity would be to search for similar bifurcations in other systems. One of the first examples of an explicit four-dimensional vector field with a heterodimensional cycle between two saddle periodic orbits is studied in [37]. This

paper also provides a numerical method for finding such cycles in other four-dimensional vector fields and for continuing them in system parameters. However, it is unclear if the heterodimensional cycle in their example is robust and how it relates to wild chaos in this system.

5 Acknowledgements

We thank Jan Kiwi for drawing our attention to the map (1) and Juan Rivera-Letelier for helpful discussions.

References

[1] Bamón R, Kiwi J, Rivera-Letelier J. Wild Lorenz-like attractors. arXiv 0508045. 2006; available at `http://arxiv.org/abs/math/0508045`.

[2] Guckenheimer J. A strange, strange attractor. In: Marsden JE, McCracken M, editors. The Hopf bifurcation theorem and its applications. New York: Springer-Verlag; 1976. p. 368–381.

[3] Guckenheimer J, Williams RF. Structural stability of Lorenz attractors. Inst Hautes Études Sci Publ Math. 1979;50(50):59–72.

[4] Afrajmovich VS, Bykov VV, Shilnikov LP. The origin and structure of the Lorenz attractor. Sov Phys Dokl. 1977;22:253–255.

[5] Afrajmovich VS, Bykov VV, Shilnikov LP. On structurally unstable attracting limit sets of Lorenz attractor type. Trans Mosc Math Soc. 1983;44:153–216.

[6] Lorenz E. Deterministic nonperiodic flow. J Atmospheric Sci. 1963;20:130–141.

[7] Asaoka M. Hyperbolic sets exhibiting C^1-persistent homoclinic tangency for higher dimensions. Proc Amer Math Soc. 2008;136(2):677–686.

[8] Asaoka M. Erratum to "Hyperbolic sets exhibiting C^1-persistent homoclinic tangency for higher dimensions". Proc Amer Math Soc. 2010;138(4):1533.

[9] Gonchenko SV, Ovsyannikov II, Simó C, Turaev D. Three-dimensional Hénon-like maps and wild Lorenz-like attractors. Internat J Bifur Chaos Appl Sci Engrg. 2005; 15(11):3493–3508.

[10] Gonchenko SV, Shilnikov LP, Turaev DV. On global bifurcations in three-dimensional diffeomorphisms leading to wild Lorenz-like attractors. Regul Chaotic Dyn. 2009; 14(1):137–147.

[11] Turaev DV, Shilnikov LP. An example of a wild strange attractor. Mat Sb. 1998; 189(1–2):291–314.

[12] Hittmeyer S, Krauskopf B, Osinga HM. Interacting global invariant sets in a planar map model of wild chaos. SIAM J Appl Dyn Syst. 2013;12(3):1280–1329.

[13] Osinga HM, Krauskopf B, Hittmeyer S. Chaos and wild chaos in Lorenz-type systems. In: AlSharawi Z, Cushing J, Elaydi S, editors. Theory and applications of difference equations and discrete dynamical systems. Berlin Heidelberg: Springer-Verlag; 2014. p. 75–98.

[14] Rovella A. The dynamics of perturbations of the contracting Lorenz attractor. Bol Soc Brasil Mat. 1993;24(2):233–259; Available from: http://dx.doi.org/10.1007/BF01237679.

[15] Keller G, StPierre M. Topological and measurable dynamics of Lorenz maps. In: Fiedler B, editor. Ergodic theory, analysis, and efficient simulation of dynamical systems. Berlin Heidelberg: Springer-Verlag; 2001. p. 333–361.

[16] Araújo V, Castro A, Pacifico MJ, Pinheiro V. Multidimensional Rovella-like attractors. J Differ Equations. 2011;251(11):3163–3201.

[17] Hittmeyer S, Krauskopf B, Osinga HM. Interactions of the Julia set with critical and (un)stable sets in an angle-doubling map on $\mathbb{C}\backslash\{0\}$. Int J Bifurcat Chaos. 2015;In print.

[18] Bunimovich LA, Sinai JG. Stochasticity of the attractor in the Lorenz model. In: Gaponov-Grekhov AV, editor. Proceedings of the winter school on nonlinear waves. Moskow: Nauka Press; 1979. p. 212–226.

[19] Sinai JG, Vul EB. Hyperbolicity conditions for the Lorenz model. Phys D. 1981; 2(1):3–7.

[20] Tucker W. The Lorenz attractor exists. C R Acad Sci Paris Sér I Math. 1999; 328(12):1197–1202.

[21] Palis J, de Melo W. Geometric theory of dynamical systems. New York: Springer-Verlag; 1982.

[22] Mira C, Gardini L, Barugola A, Cathala JC. Chaotic dynamics in two-dimensional noninvertible maps. Vol. 20 of World Sci. Ser. Nonlinear Sci. Ser. A Monogr. Treatises. Singapore: World Scientific; 1996.

[23] Dhooge A, Govaerts W, Kuznetsov YA. MatCont: a Matlab package for numerical bifurcation analysis of ODEs. ACM Trans Math Software. 2003;29(2):141–164; available at `http://sourceforge.net/projects/matcont`.

[24] Ghaziani RK, Govaerts W, Kuznetsov YA, Meijer HGE. Numerical continuation of connecting orbits of maps in Matlab. J Differ Equations Appl. 2009;15(8-9):849–875.

[25] Govaerts W, Kuznetsov YA, Khoshsiar Ghaziani R, Meijer HGE. Cl_MatContM: a toolbox for continuation and bifurcation of cycles of maps. 2008; software. Available at `http://sourceforge.net/projects/matcont`.

[26] Aronson DG, Chory MA, Hall GR, McGehee RP. Bifurcations from an invariant circle for two-parameter families of maps of the plane: a computer-assisted study. Comm Math Phys. 1982;83(3):303–354.

[27] Schilder F, Peckham BB. Computing Arnol′d tongue scenarios. J Comput Phys. 2007; 220(2):932–951.

[28] Grebogi C, Ott E, Yorke JA. Fractal basin boundaries, long-lived chaotic transients, and unstable-unstable pair bifurcation. Phys Rev Lett. 1983;50(13):935–938.

[29] Doedel EJ, Krauskopf B, Osinga HM. Global invariant manifolds in the transition to preturbulence in the Lorenz system. Indag Math. 2011;22(3-4):222–240.

[30] Doedel EJ, Krauskopf B, Osinga HM. Global organization of phase space in the transition to chaos in the Lorenz system. Preprint, The University of Auckland. 2014; available at `http://www.math.auckland.ac.nz/~berndk/transfer/dko_tochaos_prep.pdf`.

[31] Kostelich EJ, Kan I, Grebogi C, Ott E, Yorke JA. Unstable dimension variability: a source of nonhyperbolicity in chaotic systems. Phys D. 1997;109(1-2):81–90.

[32] Bonatti C, Díaz L. Robust heterodimensional cycles and C^1-generic dynamics. J Inst Math Jussieu. 2008;7(3):469–525.

[33] Gonchenko SV, Shilnikov LP, Turaev DV. On dynamical properties of multidimensional diffeomorphisms from Newhouse regions. I. Nonlinearity. 2008;21(5):923–972.

[34] Shinohara K. An example of C^1-generically wild homoclinic classes with index deficiency. Nonlinearity. 2011;24(7):1961–1974.

[35] Shinohara K. On the index problem of C^1-generic wild homoclinic classes in dimension three. Discrete Contin Dyn Syst Ser A. 2011;31(3):913–940.

[36] Bonatti C, Díaz LJ, Viana M. Dynamics beyond uniform hyperbolicity. a global geometric and probabilistic perspective. Vol. 102 of Encyclopaedia Math. Sci. Berlin: Springer-Verlag; 2005.

[37] Zhang W, Krauskopf B, Kirk V. How to find a codimension-one heteroclinic cycle between two periodic orbits. Discrete Contin Dyn Syst Ser A. 2012;32(8):2825–2851.